

Open charm production at the LHC - k_t -factorization approach

Rafał Maciula*

Institute of Nuclear Physics PAN, PL-31-342 Cracow, Poland

Antoni Szczurek†

*Institute of Nuclear Physics PAN, PL-31-342 Cracow, Poland and
University of Rzeszów, PL-35-959 Rzeszów, Poland*

(Dated: February 6, 2022)

Abstract

We discuss inclusive production of open charm in proton-proton scattering at LHC. The calculation is performed within the k_t -factorization approach. Different models of unintegrated gluon distributions (UGDF) from the literature are used. The theoretical transverse momentum as well as (pseudo)rapidity distributions of charmed mesons are compared with recent experimental data of ATLAS, ALICE and LHCb collaborations. Only the calculation with Kimber-Martin-Ryskin (KMR) UGDF gives results comparable to experimental ones. All other popular models of UGDF significantly underpredict experimental data. Several sources of uncertainties of the theoretical predictions are also studied in details. In addition we discuss correlations between D and \bar{D} mesons. Good description of experimental distribution in invariant mass and in relative azimuthal angle between D and \bar{D} mesons is achieved for the KMR UGDF. The considered correlation observables measured by the LHCb experiment were not discussed in other approaches in the literature.

PACS numbers: 13.87.Ce, 14.65.Dw

*Electronic address: rafal.maciula@ifj.edu.pl

†Electronic address: antoni.szczurek@ifj.edu.pl

I. INTRODUCTION

At high energy hadronic scattering the gluon-gluon fusion is known to be the dominant mechanism of open charm production. Even at RHIC the contribution from quark-antiquark annihilation constitutes only a small fraction of the cross section. Usually in the studies of heavy quark production the main efforts concentrate on inclusive distributions. The transverse momentum distribution of charmed mesons is the best example. Standard collinear NLO approach [1] as well as its improved schemes e.g. FONLL [2] or GM-VFNS [3] are states of art in this respect. These approaches cannot be, however, used when transverse momenta of charm quark and antiquark are not equal. This means in practice that it cannot be used for studies of correlation observables for charmed meson pairs or for meson-nonphotonic electron modes.

The k_t -factorization approach seems much more efficient tool in this respect [4–11]. Different unintegrated gluon distributions in the proton (UGDF) have been used in the literature in this context [12–16]. Recently we have applied this formalism to the description of inclusive distributions of so-called nonphotonic electrons [17] and electron-positron correlations [18] at RHIC. Rather good description of correlation observables has been achieved there.

The quark mass is sufficiently large to apply perturbative calculation, but still small enough that interesting low- x effects may appear too. In the k_t -factorization approach the latter effects are contained in the unintegrated gluon distributions – the building blocks of the formalism. In principle a comparison of experimental data and predictions with the UGDFs which include such effects may tell us more about footprints of the saturation effects – the topic extensively discussed in recent years.

Recently ATLAS [19], ALICE [20, 21] and LHCb [22] collaborations have measured inclusive distributions (mainly transverse momentum distributions) of different charmed mesons. The LHCb collaboration has measured in addition a few correlation observables for charmed mesons for the first time in the history in the forward rapidity region [23]. Before the STAR collaboration at RHIC has measured correlation of charmed mesons and nonphotonic electrons [24]. At RHIC a study of meson-meson correlations was not possible due to limited statistics caused by relatively small cross sections. It was accessible only at Tevatron where first midrapidity measurements of azimuthal angle correlations between charmed mesons have been performed by the CDF experiment [25].

In the present paper we wish to concentrate first on inclusive distributions of charmed mesons in order to test different models of unintegrated gluon distributions from the literature. Next we wish to focus on $D\bar{D}$ meson correlations. Conclusions will close our paper.

II. SKETCH OF THE FORMALISM

The cross section for the production of a pair of charm quark – charm antiquark can be written as:

$$\begin{aligned} \frac{d\sigma(pp \rightarrow c\bar{c}X)}{dy_1 dy_2 d^2p_{1t} d^2p_{2t}} &= \frac{1}{16\pi^2 \hat{s}^2} \int \frac{d^2k_{1t}}{\pi} \frac{d^2k_{2t}}{\pi} \overline{|\mathcal{M}_{g^*g^* \rightarrow c\bar{c}}^{off}|^2} \\ &\times \delta^2(\vec{k}_{1t} + \vec{k}_{2t} - \vec{p}_{1t} - \vec{p}_{2t}) \mathcal{F}_g(x_1, k_{1t}^2, \mu^2) \mathcal{F}_g(x_2, k_{2t}^2, \mu^2). \end{aligned} \quad (2.1)$$

The main ingredients in the formula are off-shell matrix elements for $g^*g^* \rightarrow c\bar{c}$ subprocess and unintegrated gluon distributions (UGDF). The relevant matrix elements are known

and can be found in Refs. [26–28]. The unintegrated gluon distributions are functions of longitudinal momentum fraction x_1 or x_2 of gluon with respect to its parent nucleon and of gluon transverse momenta k_t . Some of them depend in addition on the factorization scale μ . The longitudinal momentum fractions can be calculated as:

$$\begin{aligned} x_1 &= \frac{m_{1t}}{\sqrt{s}} \exp(y_1) + \frac{m_{2t}}{\sqrt{s}} \exp(y_2), \\ x_2 &= \frac{m_{1t}}{\sqrt{s}} \exp(-y_1) + \frac{m_{2t}}{\sqrt{s}} \exp(-y_2), \end{aligned} \quad (2.2)$$

where $m_{it} = \sqrt{p_{it}^2 + m_Q^2}$ is the transverse mass of produced quark/antiquark.

Various unintegrated gluon distributions have been discussed in the literature [12–16]. In contrast to the collinear gluon distributions (PDFs) they differ considerably among themselves. One may expect that they will lead to different production rates of $c\bar{c}$ pairs at the LHC. Since the production of charm quarks is known to be dominated by the gluon-gluon fusion, the charm production at the LHC can be used to verify the quite different models of UGDFs.

Below we wish to concentrate for a while on the Kimber-Martin-Ryskin (KMR) unintegrated gluon distribution which, as will be discussed in this paper, gives the best description of the LHC experimental data, taking into account also correlation observables.

According to the KMR approach the unintegrated gluon distribution is given by the following formula

$$\begin{aligned} f_g(x, k_t^2, \mu^2) &\equiv \frac{\partial}{\partial \log k_t^2} [g(x, k_t^2) T_g(k_t^2, \mu^2)] \\ &= T_g(k_t^2, \mu^2) \frac{\alpha_S(k_t^2)}{2\pi} \sum_b \int_x^1 dz P_{gb}(z) b\left(\frac{x}{z}, k_t^2\right). \end{aligned} \quad (2.3)$$

This definition is fully satisfied for $k_t > \mu_0$, where $\mu_0 \sim 1$ GeV is the minimum scale for which DGLAP evolution of the conventional collinear gluon distributions, $g(x, \mu^2)$, is valid.

The virtual (loop) contributions may be resummed to all orders by the Sudakov form factor,

$$T_g(k_t^2, \mu^2) \equiv \exp \left(- \int_{k_t^2}^{\mu^2} \frac{d\kappa_t^2}{\kappa_t^2} \frac{\alpha_S(\kappa_t^2)}{2\pi} \sum_b \int_0^1 dz z P_{bg}(z) \right), \quad (2.4)$$

which gives the probability of evolving from a scale k_t to a scale μ without parton emission.

The exponent of the gluon Sudakov form factor can be simplified using the following identity: $P_{qg}(1-z) = P_{qg}(z)$. Then the gluon Sudakov form factor is

$$T_g(k_t^2, \mu^2) = \exp \left(- \int_{k_t^2}^{\mu^2} \frac{d\kappa_t^2}{\kappa_t^2} \frac{\alpha_S(\kappa_t^2)}{2\pi} \left(\int_0^{1-\Delta} dz z P_{gg}(z) + n_F \int_0^1 dz P_{qg}(z) \right) \right), \quad (2.5)$$

where n_F is the quark–antiquark active number of flavours into which the gluon may split and $\Delta = k_t/(k_t + \mu)$ which introduces a restriction of the phase space for gluon emission due to the angular-ordering condition. Due to the presence of the Sudakov form factor in the KMR prescription only last emission generates transverse momentum of incoming gluons. This scheme is the direct analogy to the techniques usually applied in all standard parton

shower Monte Carlo generators. The unique feature of the KMR model of UGDF is that it provides possibility for the emission of at most one additional gluon. Therefore one can expect that the KMR model may include in an effective way NLO corrections to heavy quark production cross section.

In the literature often somewhat differently defined UGDFs are used. They differ by the following transformation:

$$\mathcal{F}_g(x, k_t^2, \mu^2) \equiv \frac{1}{k_t^2} f_g(x, k_t^2, \mu^2). \quad (2.6)$$

The normalisation condition for unintegrated distributions

$$g(x, \mu^2) = \int_0^{\mu^2} dk_t^2 f_g(x, k_t^2, \mu^2) \quad (2.7)$$

is exactly satisfied if we define

$$\left. \frac{1}{k_t^2} f_g(x, k_t^2, \mu^2) \right|_{k_t < \mu_0} = \frac{1}{\mu_0^2} g(x, \mu_0^2) T_g(\mu_0^2, \mu^2), \quad (2.8)$$

so that the density of gluons in the proton is constant for $k_t < \mu_0$ at fixed x and μ .

The precise expression for the unintegrated gluon distribution reads

$$f_g(x, k_t^2, \mu^2) = T_g(k_t^2, \mu^2) \frac{\alpha_S(k_t^2)}{2\pi} \times \int_x^1 dz \left[\sum_q P_{gq}(z) \frac{x}{z} q\left(\frac{x}{z}, k_t^2\right) + P_{gg}(z) \frac{x}{z} g\left(\frac{x}{z}, k_t^2\right) \Theta\left(\frac{\mu}{\mu + k_t} - z\right) \right]. \quad (2.9)$$

III. CHARM QUARK/ANTI-QUARK PRODUCTION AT LHC

In this section we wish to concentrate on the production of charm quarks and antiquarks. Thus this section has rather theoretical character. The cross sections for production of charmed mesons will be discussed in the next section. Before we go to the presentation of differential distributions let us summarize integrated cross sections for $c\bar{c}$ production.

Using the KMR model of unintegrated gluon distributions, the total cross section for charm quark/antiquark production at $\sqrt{s} = 7$ TeV is obtained to be $\sigma_{tot}^{KMR}(pp \rightarrow c\bar{c}X) = 7.36_{-1.77}^{+2.34}(\mu)_{-2.94}^{+6.03}(m_c)$ mb. The predicted value has large uncertainties related to the choice of factorization/renormalization scales μ and due to the charm quark mass m_c . The obtained cross section is very large, of the same order as e.g. cross section for elastic scattering or single diffraction. This means that in practice charm quark/antiquarks appear in almost each inelastic event. This is a rather new situation which requires more detailed studies.

Taking into account acceptance of ATLAS, LHCb and ALICE detectors we get $\sigma_{ATLAS}^{KMR}(pp \rightarrow c\bar{c}X) = 2.53_{-0.60}^{+0.83}(\mu)_{-0.90}^{+1.66}(m_c)$ mb, $\sigma_{LHCb}^{KMR}(pp \rightarrow c\bar{c}X) = 1.54_{-0.37}^{+0.50}(\mu)_{-0.62}^{+1.27}(m_c)$ mb and $\sigma_{ALICE}^{KMR}(pp \rightarrow c\bar{c}X) = 0.91_{-0.23}^{+0.30}(\mu)_{-0.35}^{+0.68}(m_c)$ mb, respectively. These numbers together with theoretical uncertainties are consistent with recent LHC measurements as well as with the recent FONLL [29] and GM-VFNS [30] predictions of charm cross section.

As it was mentioned in the previous section our predictions are very sensitive to the choice of unintegrated gluon distributions. Different UGDFs are very often based on quite different

theoretical assumptions. This has a crucial meaning for their kinematical characteristics. In Fig. 1 we show dependence of the unintegrated gluon distributions functions on gluon transverse momentum squared k_t^2 for several values of x relevant for the production of charm quarks and antiquarks at LHC energy. Differences in shapes in k_t^2 of the plotted functions are significant. One can also see different dependence on x of the different considered UGDFs. Changing the value of x , the mutual trends between them also change what makes the overall picture more complicated. Especially the KMR model seems to reveal the strongest x -dependence.

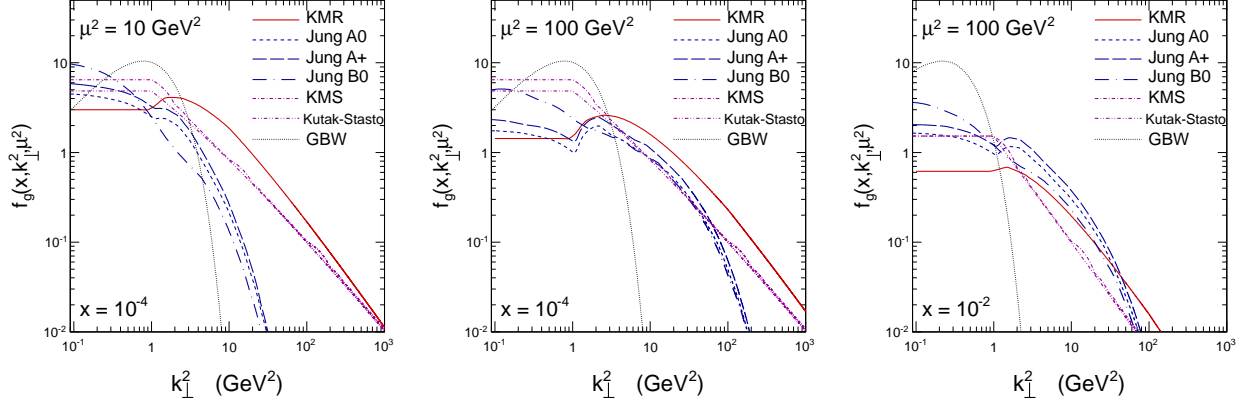


FIG. 1: Different unintegrated gluon distributions from the literature as a function of gluon transverse momentum squared k_t^2 for different values of longitudinal momentum fraction x of the gluon initiating the hard process and for different factorization scale μ .

The rapidity of the quark or antiquark are strongly correlated with longitudinal momentum fractions of gluons initiating the hard process. This is shown in Fig. 2 for the KMR UGDF. At rapidities $|y| > 5$ one starts to probe longitudinal momentum fractions smaller than 10^{-4} . This is a new situation compared to earlier measurements at RHIC or Tevatron. The unintegrated gluon distributions (UGDFs) as well as standard collinear ones (PDFs) were not tested so far in this region.

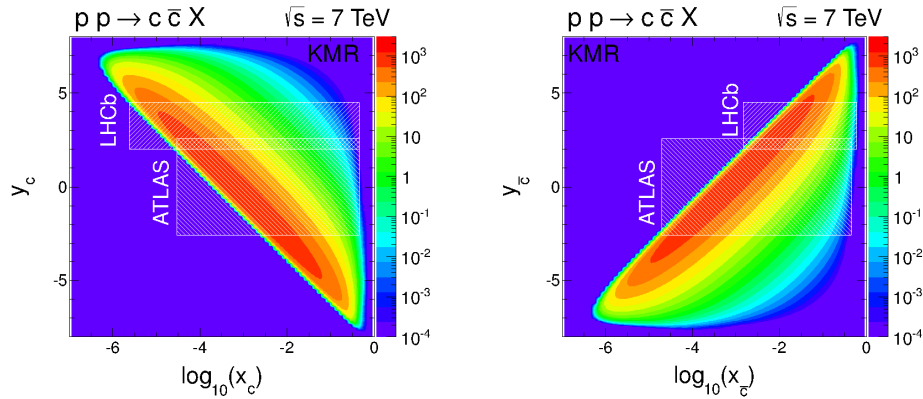


FIG. 2: The range of longitudinal momentum fraction of gluons and its correlation to the rapidity of charm quark (left) or antiquark (right). In addition regions of the coverage for the ATLAS and LHCb experiments are shown.

It was advocated in Ref. [31] that the two-dimensional distribution in transverse momentum of charm quark and charm antiquark can be a good "theoretical observable" to study unintegrated gluon distributions. In Fig. 3 we show such distributions for different UGDFs from the literature. We use here KMR [12], KMS [13], Kutak-Stasto [14], Jung setA+, setB+ [15] and GBW [16] parametrizations. Quite different pattern is obtained for different UGDFs. This may have direct consequences for correlation observables for mesons or/and nonphotonic electrons. Moreover, events when one p_t is small and second one is large correspond to the region relevant for higher order collinear corrections. It is clear from this $p_{1t}p_{2t}$ -plane that effects of an effective inclusion of NLO diagrams in the k_t -factorization approach strongly depend on the construction of UGDFs.

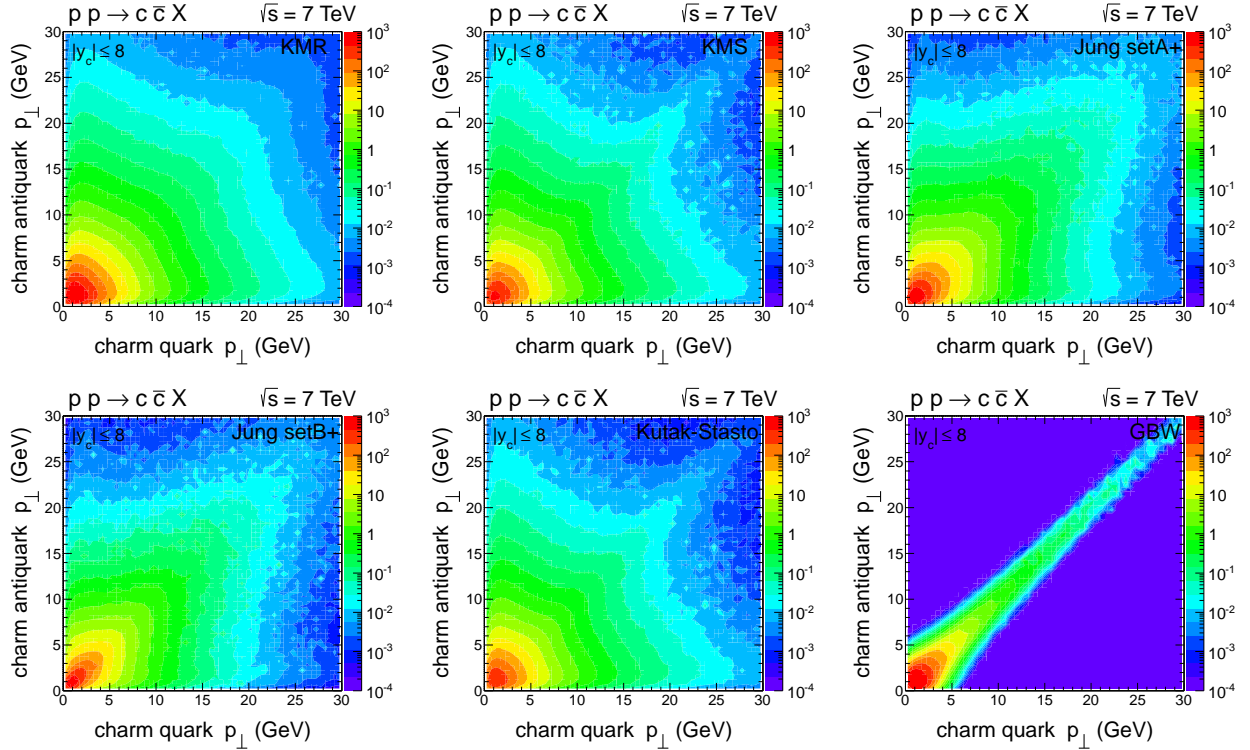


FIG. 3: Two dimensional maps in transverse momentum of charm quark and transverse momentum of the charm antiquark for different unintegrated gluon distributions.

The production of charmed mesons strongly depends on the choice of UGDF model as will be discussed in the next section. As will become clear there the KMR UGDF within rather large theoretical uncertainties provides the best description of the LHC experimental data. The major part of these uncertainties comes from the perturbative part of the calculation. Therefore in the following we wish to spend some time to define uncertainties of the corresponding calculations at the quark level. In Fig. 4 and Fig. 5 we present the uncertainties of our predictions, obtained by changing charm quark mass $m_c = 1.5 \pm 0.3$ GeV and by varying renormalization and factorization scales $\mu^2 = \zeta m_t^2$, where $\zeta \in (0.5; 2)$. The gray shaded bands represent these both sources of uncertainties summed in quadrature. The smaller transverse momentum the larger uncertainty. For comparison we show also results for the FONLL [2] and MC@NLO (denoted on figures as NLO PM) [32] approaches. Our result of the k_t -factorization approach is consistent within the uncertainty bands with those rather standard NLO collinear calculations. Only at small quark p_t 's some difference

appears. This is the region where transverse momenta of incident gluons play an important role. Particularly, a detailed treatment of the nonperturbative k_t region in UGDF may lead to a dumping or an enhancement of the cross section at small p_t .

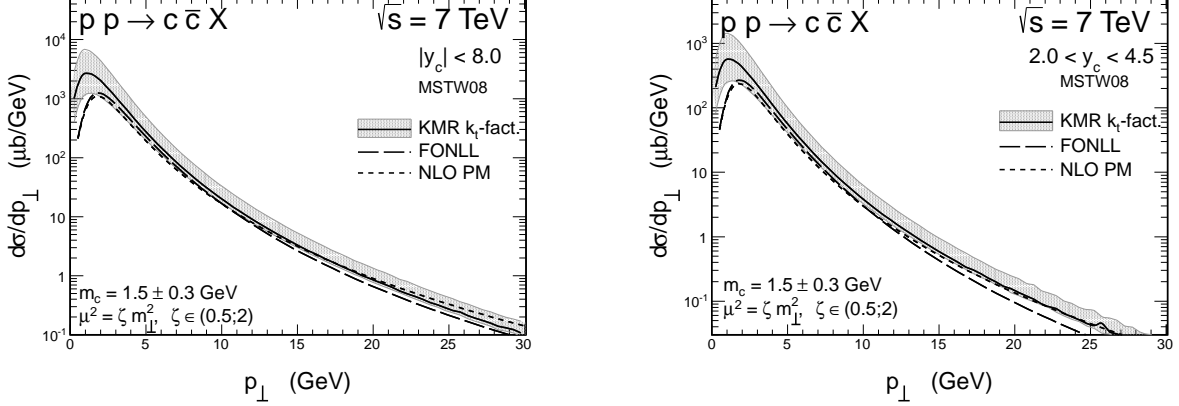


FIG. 4: Theoretical uncertainties on transverse momentum distribution of c or \bar{c} production due to the choice of factorization/renormalization scale and those related to charm quark mass for the KMR UGDF (solid line with the shaded bands). Left panel shows the cross section for the whole range of quark/antiquark rapidities while the left panel for the rapidity range relevant for the LHCb experiment. For comparison the FONLL and NLO PM predictions are also shown.

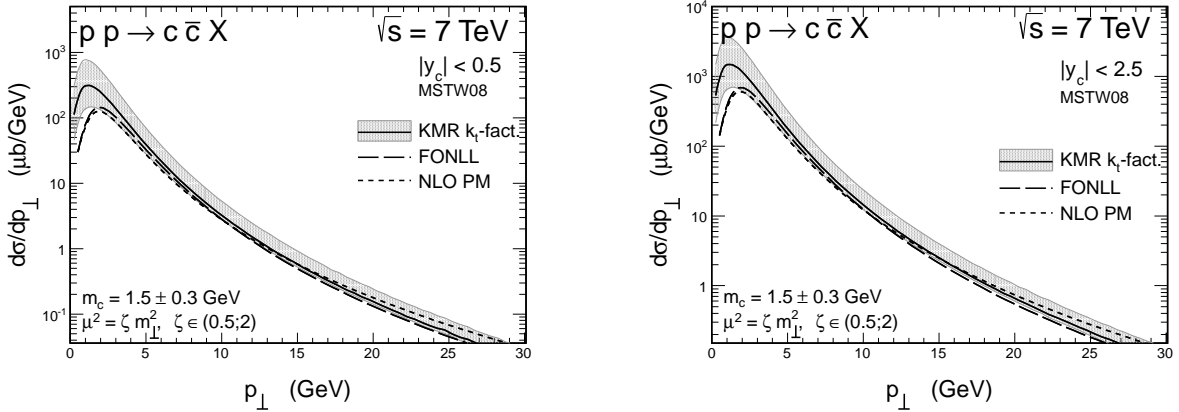


FIG. 5: The same as in Fig.4 but for the ALICE (left panel) and ATLAS or CMS (right panel) kinematics.

IV. PRODUCTION OF CHARMED MESONS

The hadronization of heavy quarks is usually done with the help of fragmentation functions. The inclusive distributions of charmed mesons can be obtained through a convolution

of inclusive distributions of charm quarks/antiquarks and $c \rightarrow D$ fragmentation functions:

$$\frac{d\sigma(pp \rightarrow D\bar{D}X)}{dy_D d^2p_{t,D}} \approx \int_0^1 \frac{dz}{z^2} D_{c \rightarrow D}(z) \frac{d\sigma(pp \rightarrow c\bar{c}X)}{dy_c d^2p_{t,c}} \bigg|_{\substack{y_c=y_D \\ p_{t,c}=p_{t,D}/z}}, \quad (4.1)$$

where $p_{t,c} = \frac{p_{t,D}}{z}$ and z is the fraction of longitudinal momentum of heavy quark carried by meson. We have made typical approximation assuming that y_c is unchanged in the fragmentation process, i.e. $y_D = y_c$.

As a default set in our calculations we use standard Peterson model of fragmentation function [33] with the parameter $\varepsilon_c = 0.05$. This value was extracted by ZEUS and H1 analyses and seems to be relevant for LO calculations. However, in the fragmentation scheme applied in the FONLL framework, rather harder functions (or smaller ε_c) are suggested [34]. This issue together with effects of applying other fragmentation functions from the literature [35–37] will be discussed in more detail when discussing differential distributions.

In Table I we have collected integrated cross sections for the production of different species of D mesons. Measured cross sections from different LHC experiments are compared to theoretical predictions obtained with three sets of UGDFs. The error bars shown for the KMR UGDF reflect uncertainty due to the choice of factorization/renormalization scale (μ) and related to the mass of the quark (m_c). The fractional uncertainties due to these both sources for other UGDFs are similar. Only cross sections obtained with the KMR UGDF are consistent within error bars with the experimental data.

In the cases of measurements with the full coverage of the meson transverse momentum range, the theoretical cross sections are almost insensitive to the fragmentation model. Quite different situation is observed when small p_t region is excluded. In the latter case, using the Peterson model with $\varepsilon_c = 0.02$ (which gives results closer to the FONLL predictions) we note the enhancement of the integrated cross sections by about 20%.

Let us start presentation of differential distributions for different LHC experiments.

A. ALICE

Let us focus first on the production of charmed mesons at midrapidities. The ALICE collaboration has performed a measurement of transverse momentum distribution of D^0 , D^+ , D^{*+} , D_s^+ [20, 21]. In the very limited range of (pseudo)rapidity one tests unintegrated gluon distributions in a pretty narrow region of longitudinal momentum fractions (see Fig. 2). In Fig. 6 we show transverse momentum distribution of D^0 mesons. In the left panel we present results for different UGDF known from the literature. Most of the existing distributions fail to describe the ALICE data. The KMR UGDF provides the best description of the measured distributions. Therefore in the following we shall concentrate on the results obtained with the KMR UGDF. In the right panel we show uncertainties due to the choice of usual integrated collinear gluon distributions (PDFs) used for calculating the KMR UGDF. In the latter case the biggest uncertainty can be observed at small transverse momenta, i.e. in the region of small gluon longitudinal momentum fraction. We use rather up-to-date MSTW08 [38], CTEQ6 [39] and GJR08 [40] parametrizations as well as GRV94 [41] which is fairly older but was very often used in last years in similar analyzes. For more detailed discussion of the PDFs aspects in charm production we refer the reader to Ref. [42]. In Fig. 7 we show separately uncertainties due to the choice of factorization/renormalization scale (left panel)

TABLE I: Integrated cross sections for production of different D mesons at LHC.

Acceptance	Mode	$\sigma_{tot}^{EXP} [\mu\text{b}]$	$\sigma_{tot}^{THEORY} [\mu\text{b}]$		
			KMR ${}^{\pm}(\mu)$ ${}^{\pm}(m_c)$	Jung setA0+	KMS
ALICE	$(D^0 + \bar{D}^0)/2$	$516 \pm 41^{+69}_{-175}$	$514^{+169}_{-130} {}^{+384}_{-198}$	317	313
$ y < 0.5$	$(D^+ + D^-)/2$	$248 \pm 30^{+52}_{-92}$	$206^{+68}_{-52} {}^{+154}_{-79}$	127	125
	$(D^{*+} + D^{*-})/2$	$247 \pm 27^{+36}_{-81}$	$208^{+69}_{-53} {}^{+156}_{-80}$	129	127
ALICE					
$ y < 0.5$	$(D_S^+ + D_S^-)/2$	$53 \pm 12^{+13}_{-15}$	$20^{+5}_{-4} {}^{+7}_{-5} (+20\%)$	13 (+20%)	13 (+20%)
$2 < p_\perp < 12 \text{ GeV}$					
LHCb	$D^0 + \bar{D}^0$	1488 ± 182	$1744^{+565}_{-418} {}^{+1435}_{-700}$	1162	872
$2 < y < 4.5$	$D^+ + D^-$	717 ± 109	$697^{+226}_{-167} {}^{+574}_{-280}$	465	349
$0 < p_\perp < 8 \text{ GeV}$	$D^{*+} + D^{*-}$	676 ± 137	$705^{+229}_{-169} {}^{+582}_{-284}$	471	354
	$D_S^+ + D_S^-$	194 ± 38	$246^{+80}_{-59} {}^{+203}_{-99}$	164	123
ATLAS	$D^+ + D^-$	$238 \pm 13^{+35}_{-23}$	$137^{+31}_{-20} {}^{+30}_{-24} (+20\%)$	103 (+20%)	93 (+20%)
$ \eta < 2.1$	$D_S^+ + D_S^-$	$168 \pm 34^{+27}_{-25}$	$48^{+12}_{-7} {}^{+11}_{-8} (+20\%)$	36 (+20%)	33 (+20%)
$p_\perp > 3.5 \text{ GeV}$	$D^{*+} + D^{*-}$	$285 \pm 16^{+32}_{-27}$	$155^{+37}_{-22} {}^{+37}_{-28} (+20\%)$	115 (+20%)	104 (+20%)

and those due to the choice of the quark mass (right panel). The uncertainties due to the choice of scales is rather large. The uncertainties due to quark mass are significant only at small transverse momenta. They are calculated by varying the quark mass $m_c = 1.5 \pm 0.3 \text{ GeV}$ and are representative for all other UGDFs.

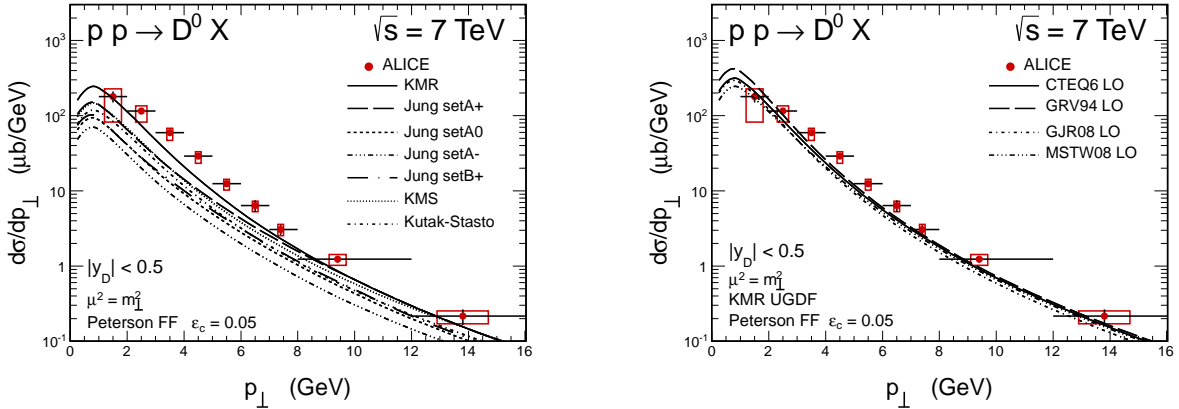


FIG. 6: Transverse momentum distribution of D^0 mesons for the ALICE measurement. The left panel shows results for different UGDFs while the right panel shows uncertainties due to the choice of collinear gluon distributions in calculation of the KMR UGDF.

In Fig. 8 and Fig. 9 we present corresponding plots for D^+ mesons. The situation here is very similar to the case of D^0 mesons.

Let us quantify now uncertainties due to the fragmentation process. Fig. 10 shows results for D^0 (left panel) and D^+ (right panel) mesons for different fragmentation functions from

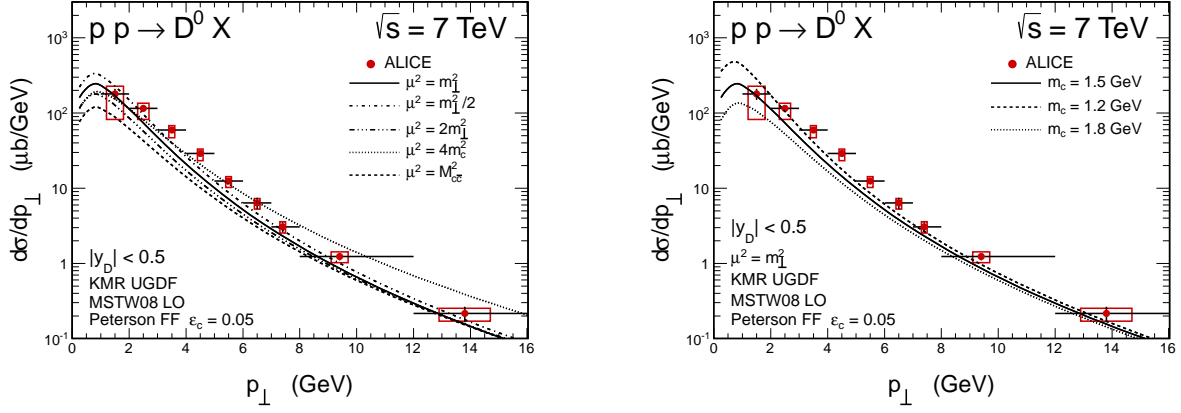


FIG. 7: Uncertainties of the theoretical cross section for the D^0 meson production within the ALICE acceptance due to the choice of the scale (left) and due to the quark mass (right).

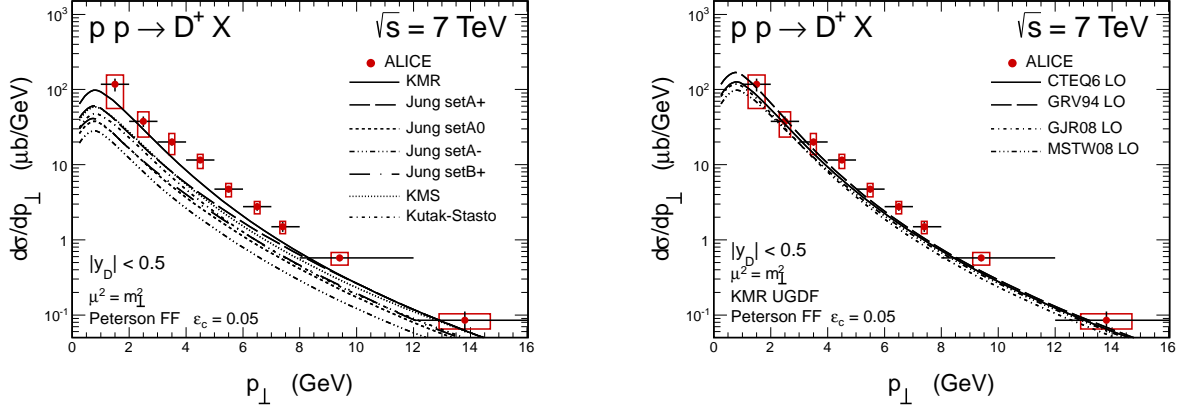


FIG. 8: The same as in Fig. 6 but for the production of D^+ mesons.

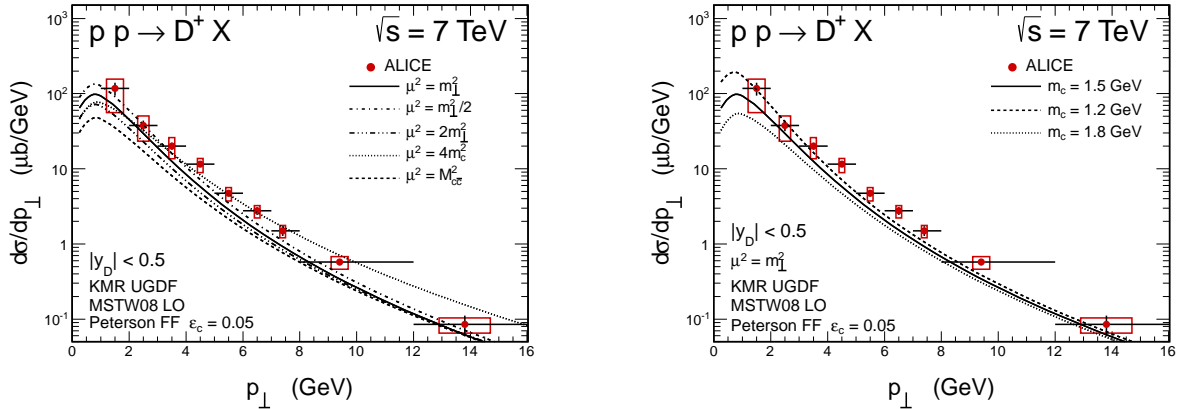


FIG. 9: The same as in Fig. 7 but for the D^+ meson.

the literature. We use here the Peterson model with three different sets of ε_c parameter, as well as Braaten et al. [35], Kartvelishvili et al. [36] and Collins-Spiller [37] parametrizations.

All of the applied functions give similar results. The effects related to the fragmentation process seem to be important only at larger meson p_t 's, starting from $p_t = 3$ GeV.

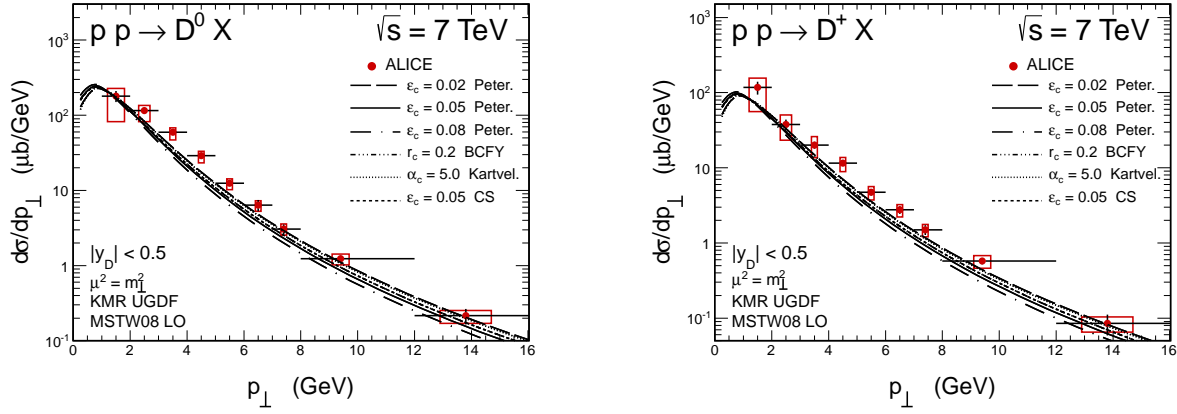


FIG. 10: Uncertainties due to fragmentation parameter ε_c in the Peterson fragmentation function and related to the choice of other fragmentation models for the KMR UGDFs.

Let us compare now results of our approach to the results of some other popular approaches used in the literature. In Fig. 11 and Fig. 12 we present such a comparison. Our results obtained within the k_t -factorization approach with the KMR UGDF are very similar to those obtained within NLO PM and FONLL models. The cross sections obtained within leading-order collinear approximation (LO PM) are much smaller, in particular for larger transverse momenta. Comparing left and right panels of these figures one can observe an improvement of the large p_t data description when $\varepsilon_c = 0.02$ in the Peterson function is taken. This choice corresponds to the upper limit of our uncertainties in the hadronization. It makes our results closer to those from FONLL. In the FONLL approach as a default fragmentation scheme for charm quarks the BCFY model with $r_c = 0.1$ is used. However, the Peterson parametrization with $\varepsilon_c = 0.02$ gives in general very similar characteristics. Since our k_t -factorization calculation is very similar to the FONLL predictions at the quark level (see Fig. 5) application of the harder fragmentation functions may be justified.

Now let us consider for the moment distributions for vector mesons D^{*+} . In Fig. 13 we show transverse momentum distributions of D^{*+} for different UGDFs and uncertainties in calculating distributions with the KMR UGDF due to the choice of collinear gluon distributions. As in the previous cases, the choice of collinear PDFs has some importance only at small transverse momenta. The same conclusions as in the cases of pseudoscalar mesons come from Fig. 14, where uncertainties due to the scales (left) and related to the quark mass (right) are presented. In Fig. 15 both of these sources are taken together and our predictions with the KMR UGDF are confronted once again with LO and NLO PM collinear calculations. Here we use the Braaten et al. model for fragmentation which has, the only one on the market, parametrization of fragmentation function for the transition of heavy quark into vector meson state.

Finally in Fig. 16 we show distributions for D_s^+ mesons, i.e. mesons built of charm and strange quarks/antiquarks. The corresponding cross section is considerably smaller than for the charm mesons containing light (up or down) quarks/antiquarks. The general situation is, however, very similar. The KMR UGDF provides the best agreement with the ALICE data. Results for other UGDFs are much below the experimental data which means, in our

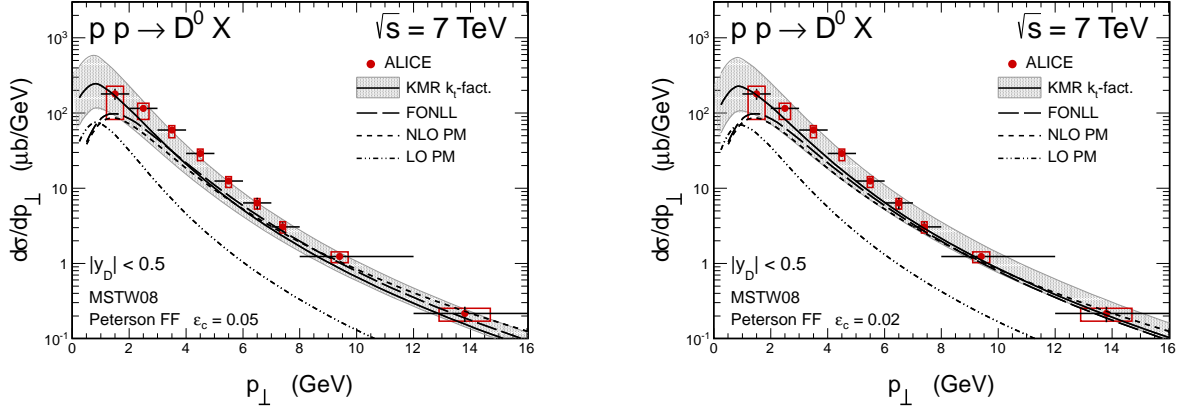


FIG. 11: Transverse momentum distribution of D^0 mesons for the ALICE kinematical region for different values of the Peterson ε_c parameter. Together with our predictions for the KMR UGDF (solid line with shaded band) results of different popular approaches are also shown.

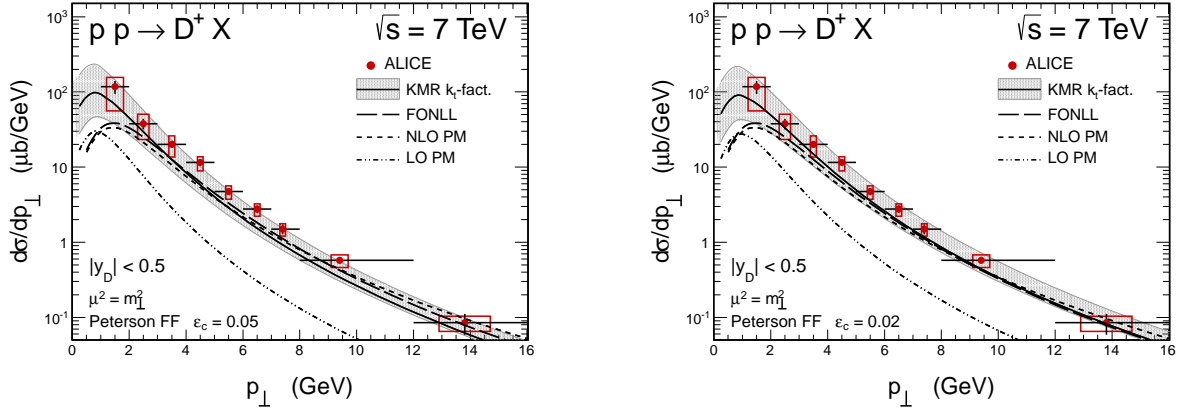


FIG. 12: The same as in Fig. 11 but for the D^+ meson.

opinion, that they do not pass the powerfull test. In the case of D_S^+ meson a different, quite important source of uncertainties appears, namely the poorly known fragmentation fractions $\text{BR}(c \rightarrow D_S^+)$. Changing the value from 0.08 (ZEUS, H1) to 0.116 (ALEPH) a significant enhancement of the theoretical predictions is achieved.

B. ATLAS

The ATLAS experiment covers much broader range of pseudorapidities than ALICE. As a consequence one tests broader region of longitudinal momentum fractions $10^{-4} < x_1, x_2 < 10^{-2}$. The gluon distributions in this range of x_1 and x_2 values carried by gluons are rather well known. Also application of the known UGDFs from the literature should be reliable.

Fig. 17 shows transverse momentum distributions of charged pseudoscalar D^\pm mesons for different models of unintegrated distributions, for $\varepsilon_c = 0.05$ (left) and $\varepsilon_c = 0.02$ (right). General situation is very similar as for the ALICE experiment although the agreement is somewhat worse. Only the upper limit of the KMR result is compatible with the ATLAS

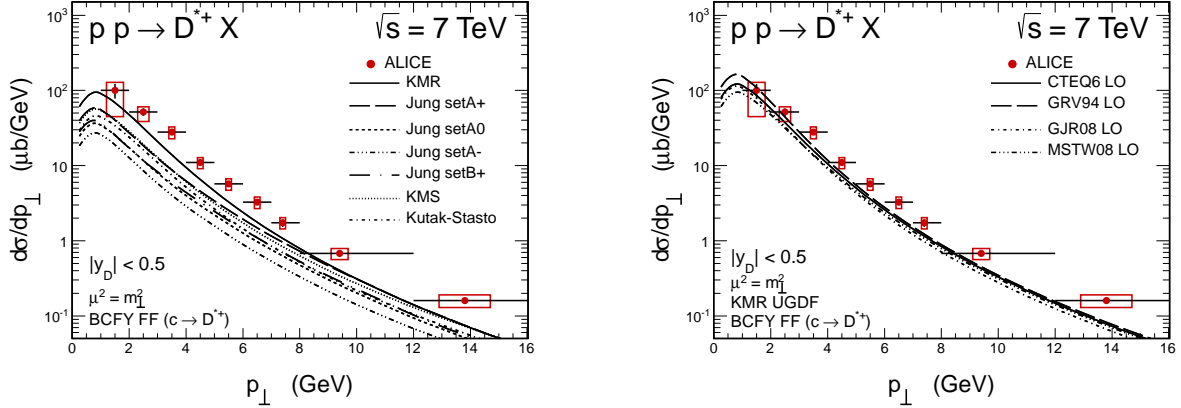


FIG. 13: Transverse momentum distribution of D^{*+} mesons for different UGDFs (left) and the uncertainties due to the choice of collinear PDFs used in calculating the KMR UGDF (right).

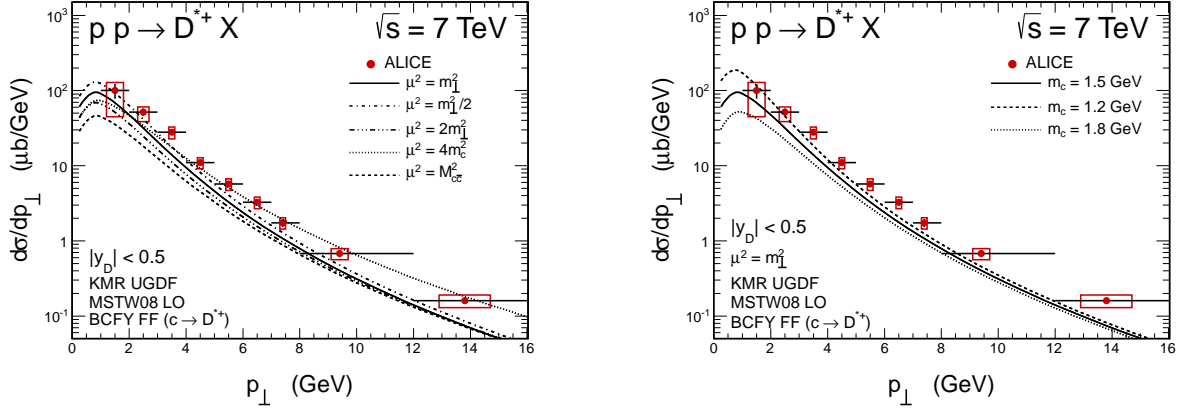


FIG. 14: Transverse momentum distribution of D^{*+} mesons. Shown are uncertainties due to the choice of scales in the KMR UGDF (left panel) and due to the quark masses (right panel).

experimental data. This may be caused by much broader range of pseudorapidities in the case of the ATLAS detector. Potentially, this can be related to double-parton scattering effects to be discussed elsewhere [43]. Also the other standard approaches give results below the ATLAS data as can be seen in Fig. 18.

Due to fairly large span of pseudorapidities the ATLAS collaboration can extract also pseudorapidity distributions. We wish to show now also results for charm meson pseudorapidity distributions. In Fig. 19 and Fig. 20 we show pseudorapidity distributions for charged D^\pm meson. These distributions are rather flat. The results are also compared to recent (preliminary) ATLAS data. Only the upper limits of large error bars of the theoretical results obtained with the KMR distributions are consistent with the ATLAS data. The results with other UGDFs clearly underpredict the experimental data.

As for pseudoscalar mesons above, in Fig. 21 we show transverse momentum distributions for charged vector mesons. The situation is pretty much the same as for pseudoscalar charged mesons discussed previously in Figs. 17 and Fig. 18.

In Fig. 20 we compare results obtained within the k_t -factorization approach (grey band)

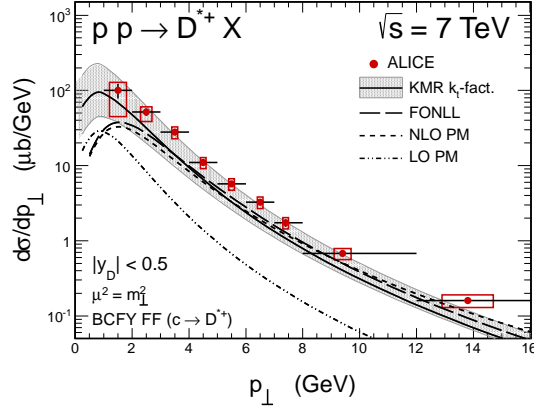


FIG. 15: Transverse momentum distribution of D^{*+} mesons for different approaches known from the literature. The grey band represents overall uncertainties of the k_t -factorization approach with the KMR UGDF.

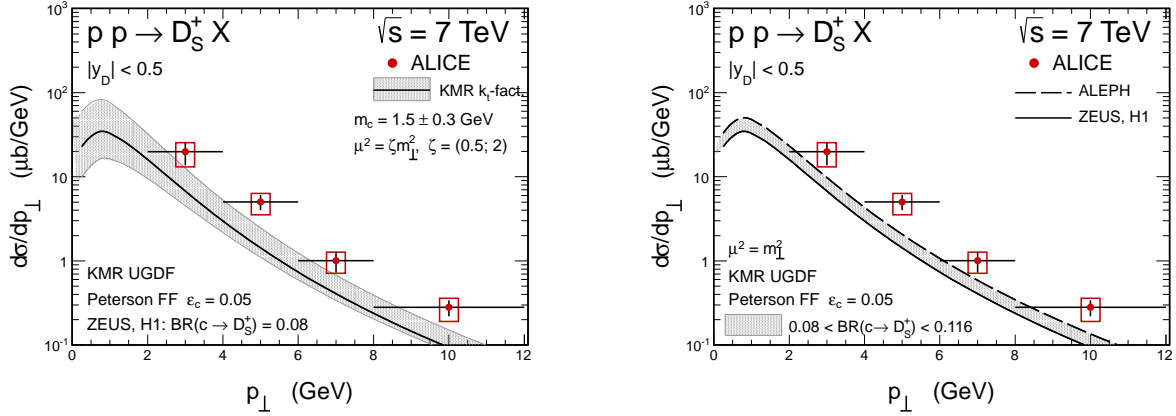


FIG. 16: Transverse momentum distribution of D_s^+ mesons. We show uncertainties due to the choice of scales and masses (left panel) and uncertainties related to poorly known fragmentation branching fraction $\text{BR}(c \rightarrow D_s^+)$ (right panel).

with results obtained within other approaches. The central value of the k_t -factorization approach with the KMR UGDF is consistent with the FONLL and NLO PM predictions.

C. LHCb

Finally let us focus on the measurements in the forward rapidity region $2 < y < 4.5$. Recently the LHCb collaboration presented first results for the production of D^0 , D^+ , D^{*+} and D_s^+ mesons [22]. In this region of phase space one tests asymmetric gluon longitudinal momentum fractions: $x_1 \sim 10^{-5}$ and $x_2 > 10^{-2}$ (see Fig. 2). This is certainly more difficult region for reliable calculation and interpretation of experimental data. First of all gluon distributions were never tested at such small x_1 values. Secondly many UGDFs from the literature may be not good enough for $x_2 > 10^{-2}$. Therefore some care in interpreting the results is required.

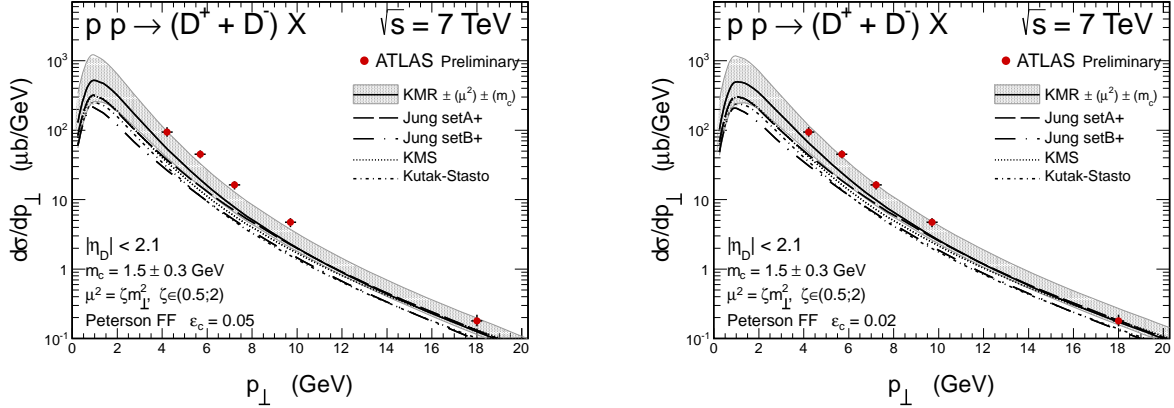


FIG. 17: Transverse momentum distribution of D^\pm mesons for different UGDFs from the literature compared with the preliminary ATLAS experimental data for $\varepsilon_c = 0.05$ (left) and $\varepsilon_c = 0.02$ (right).

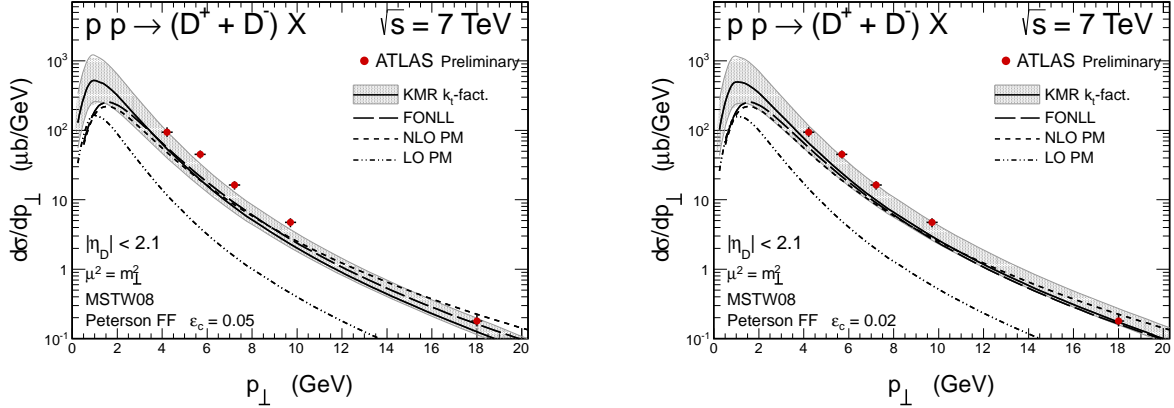


FIG. 18: Transverse momentum distribution of D^\pm mesons for different standard approaches compared with the ATLAS experimental data [19] for $\varepsilon_c = 0.05$ (left) and $\varepsilon_c = 0.02$ (right). The details are specified in the figures.

The LHCb, similar as ALICE, has measured also distributions of rather rarely produced D_s^\pm mesons. We start from transverse momentum distributions for D_s^\pm mesons. In Fig. 22 we present distributions for different UGDF from the literature and uncertainties for the KMR UGDF related to the choice of standard PDFs. In Fig. 23 we show uncertainties related to the choice of factorization/renormalization scale and due to the choice of quark masses and in Fig. 24 uncertainties related to fragmentation functions. All these uncertainties are very similar as for the ALICE and ATLAS kinematics.

In Fig. 25 we compare our predictions, together with predictions of other popular approaches. Main conclusions are the same again as for the ALICE and ATLAS.

The LHCb collaboration was able to measure transverse momentum distributions of mesons in many narrow bins of (pseudo)rapidity. Below (Figs. 26, 27 and 28) we show such distributions for D^0 , D^+ and D^{*+} , respectively. In general, different bins are sensitive to different regions of longitudinal momentum fractions carried by gluons. However, we do not observe any interesting trend in the quality of the description of the LHCb data. Our

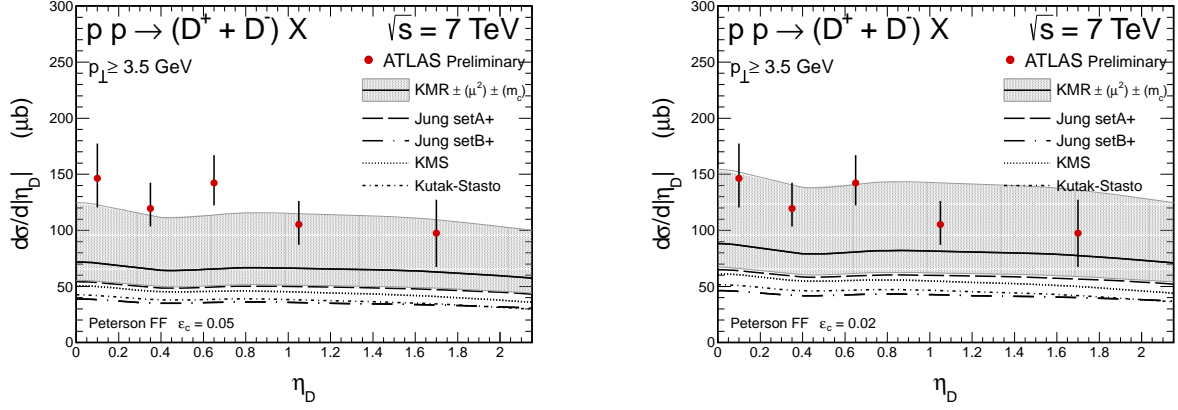


FIG. 19: Distribution in D^\pm meson pseudorapidity. The results for different UGDFs are compared with the ATLAS preliminary data [19] for different values of the parameter ε_c of the Peterson fragmentation function: $\varepsilon_c = 0.05$ (left), $\varepsilon_c = 0.02$ (right).

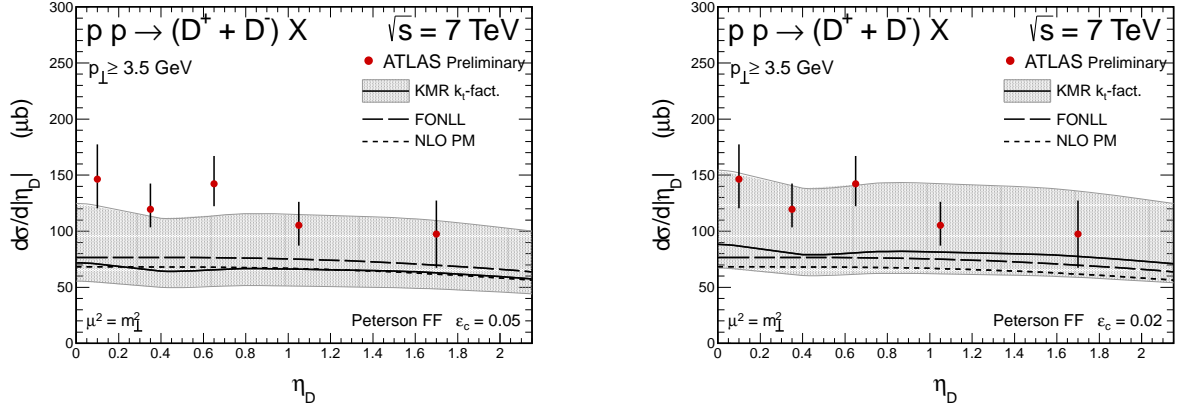


FIG. 20: Distribution in D^\pm meson pseudorapidity. The results of our calculation are compared with those for other calculations and with the ATLAS preliminary data [19] for different values of the parameter ε_c of the Peterson fragmentation function: $\varepsilon_c = 0.05$ (left), $\varepsilon_c = 0.02$ (right).

results with the KMR UGDF within uncertainties are consistent with the experimental data and with the FONLL and NLO PM predictions. Corresponding distributions for PYTHIA are taken from Ref. [22] and have slightly different p_t -slope than the other ones.

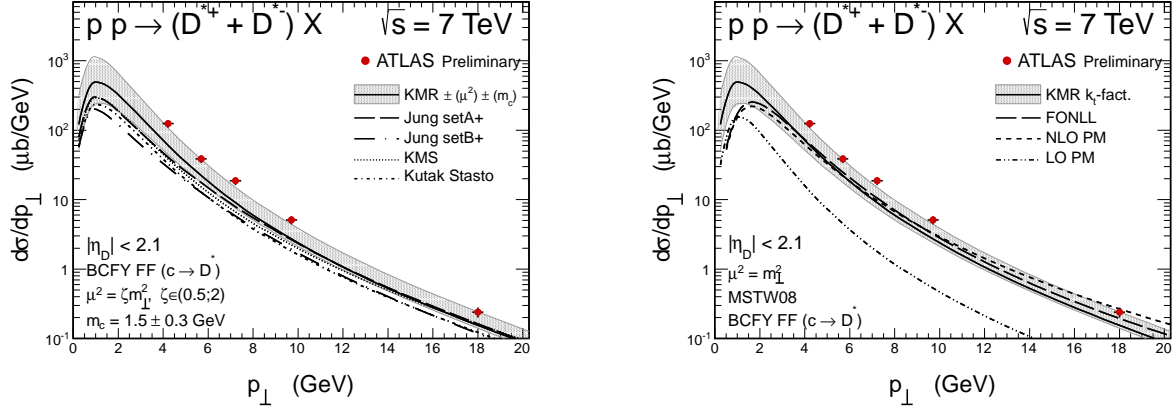


FIG. 21: Distribution in D^{*+} meson transverse momentum. The results of our calculation are compared with the ATLAS preliminary data [19]. In the left panel we show results for different UGDFs and in the right panel our results are compared with other approaches.

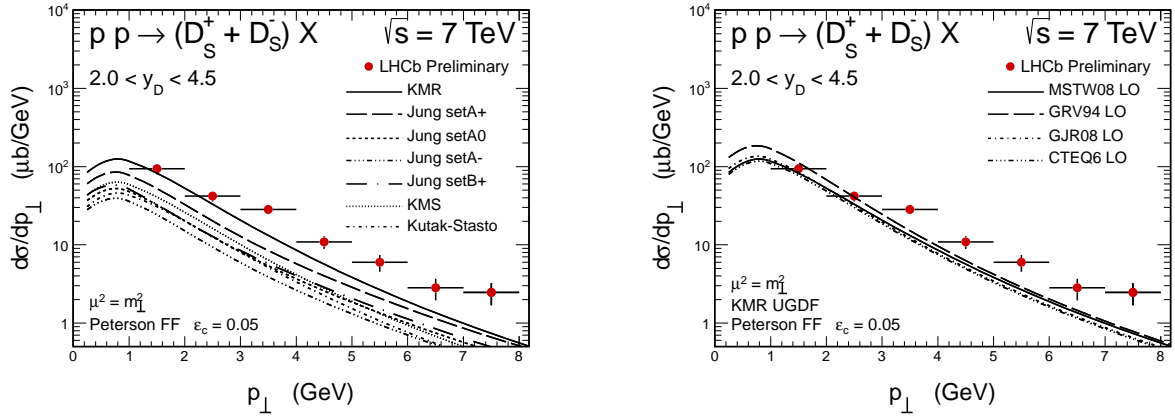


FIG. 22: Transverse momentum distribution of D_s^\pm mesons for different UGDFs from the literature (left) and the dependence on the choice of collinear gluon distribution functions for the KMR UGDF (right). The results of calculation are compared with the LHCb collaboration data.

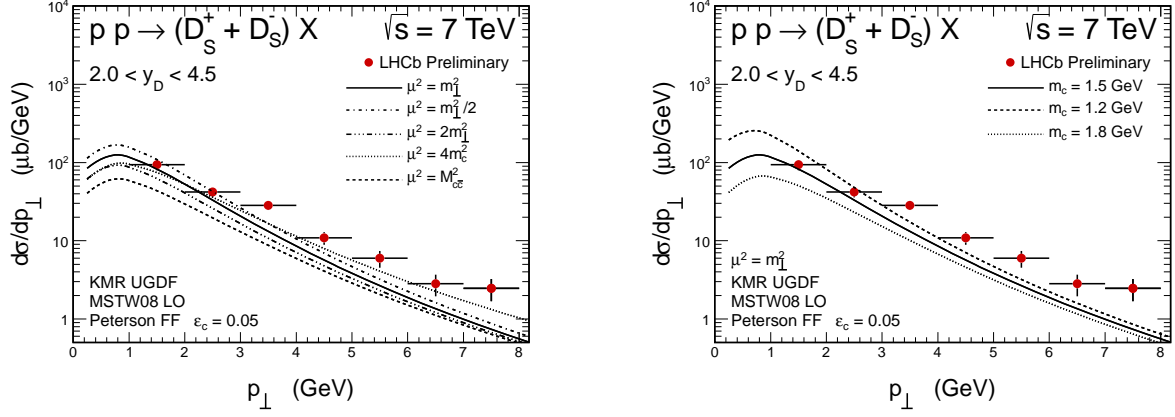


FIG. 23: Uncertainties of the theoretical predictions due to the choice of scales for the KMR UGDF (left) and due to charm quark mass (right).

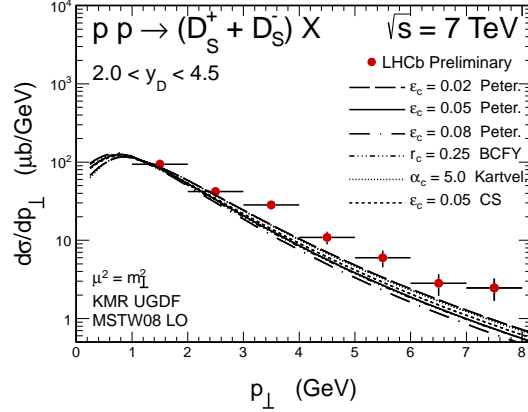


FIG. 24: Uncertainties in the fragmentation of $c \rightarrow D_s^+$. We show results obtained with different fragmentation functions from the literature.

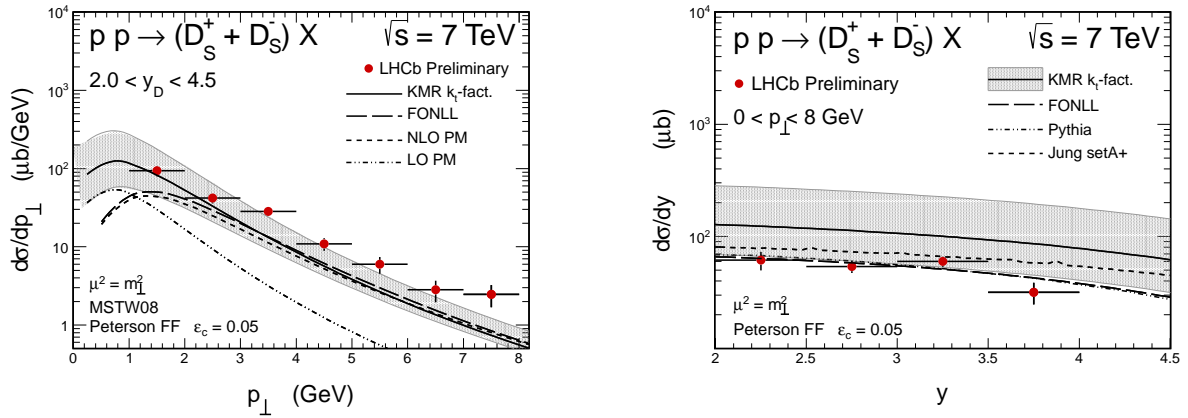


FIG. 25: Results with overall uncertainties for transverse momentum (left) and rapidity distributions (right) of D_s^\pm for the k_t -factorization approach with the KMR UGDF. For comparison we show predictions of other popular approaches.

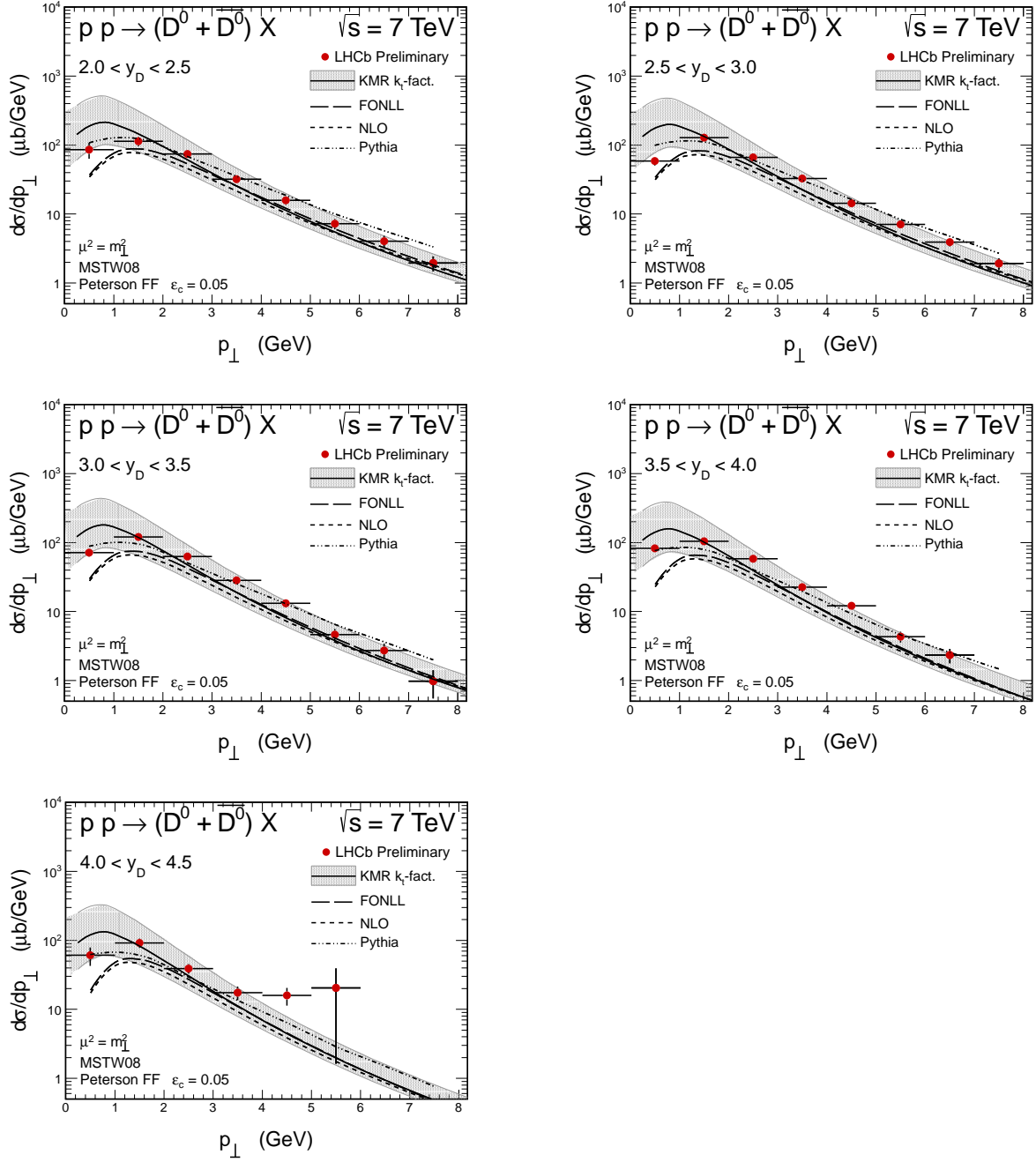


FIG. 26: Transverse momentum distribution of neutral D^0 mesons for different ranges of rapidities specified in the figures. We compare results of the k_t -factorization approach with the KMR UGDF and those obtained within other approaches known from the literature.

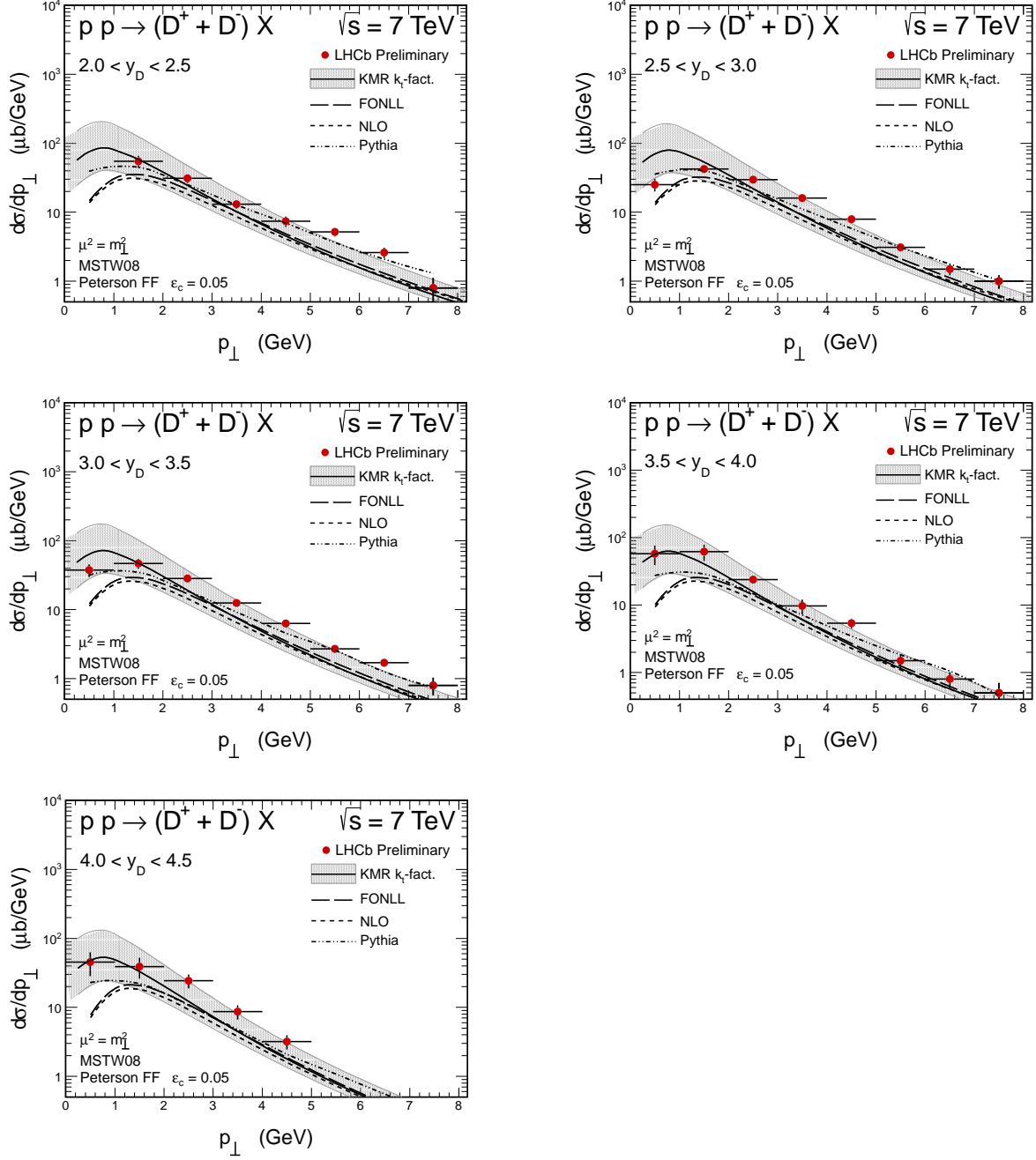


FIG. 27: Transverse momentum distribution of charged D^+ mesons for different ranges of rapidities specified in the figures. We compare results of the k_t -factorization approach with the KMR UGDF and those obtained within other approaches known from the literature.

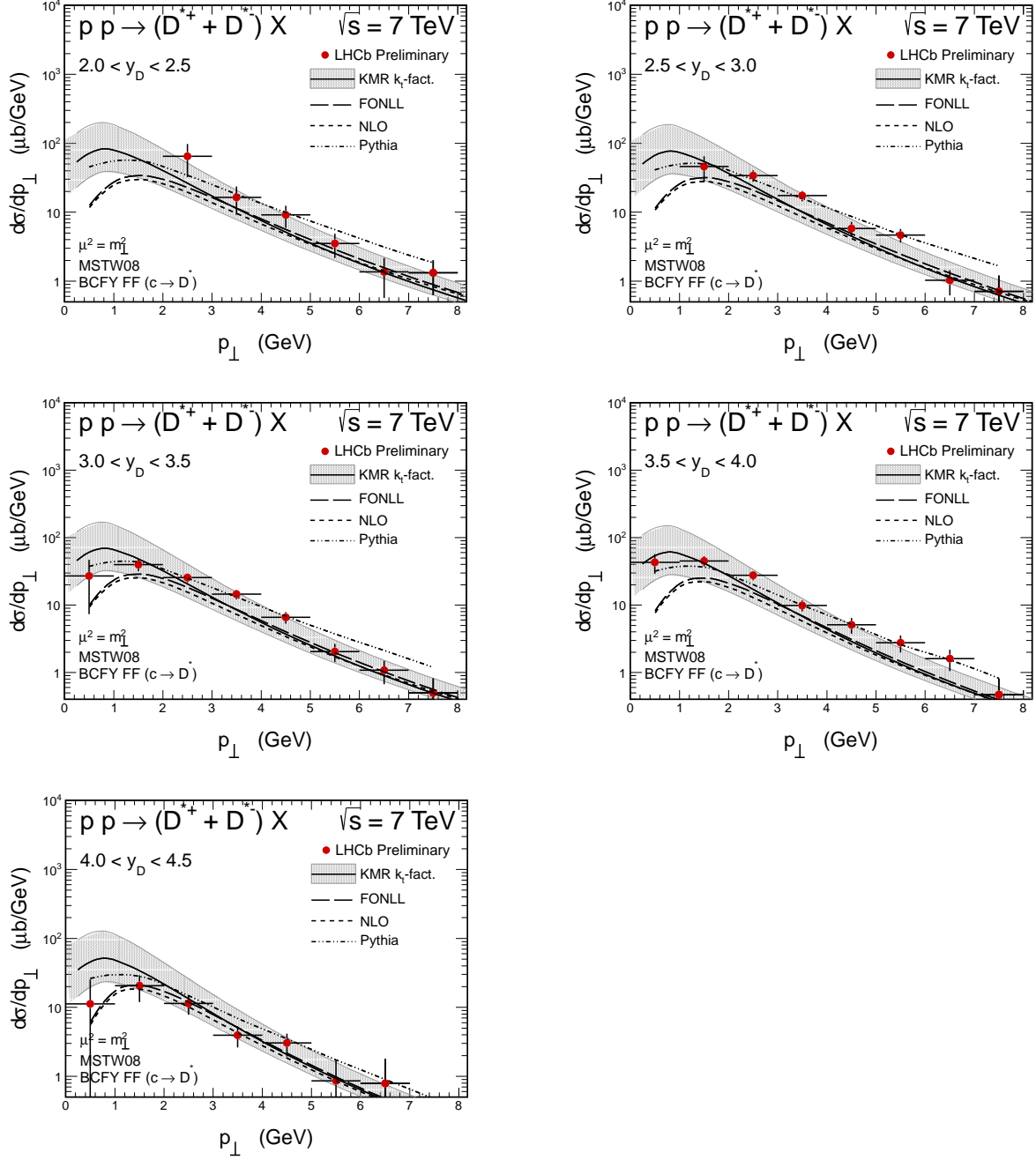


FIG. 28: Transverse momentum distribution of D^{*+} mesons for different ranges of rapidities specified in the figures. We compare results of the k_t -factorization approach with the KMR UGDF and those obtained within other approaches known from the literature.

V. PRODUCTION OF $D\bar{D}$ PAIRS

Most of the calculations in the literature concentrates on single meson distributions. We wish to focus now on correlation observables for D and \bar{D} mesons. In order to calculate correlation observables for two mesons we follow here, similar as in the single meson case, the fragmentation function technique for hadronization process:

$$\frac{d\sigma(pp \rightarrow D\bar{D}X)}{dy_1 dy_2 d^2 p_{1t}^D d^2 p_{2t}^{\bar{D}}} \approx \int \frac{D_{c \rightarrow D}(z_1)}{z_1} \cdot \frac{D_{\bar{c} \rightarrow \bar{D}}(z_2)}{z_2} \cdot \frac{d\sigma(pp \rightarrow c\bar{c}X)}{dy_1 dy_2 d^2 p_{1t}^c d^2 p_{2t}^{\bar{c}}} dz_1 dz_2, \quad (5.1)$$

where: $p_{1t}^c = \frac{p_{1t}^D}{z_1}$, $p_{2t}^{\bar{c}} = \frac{p_{2t}^{\bar{D}}}{z_2}$ and meson longitudinal fractions $z_1, z_2 \in (0, 1)$. The multidimensional distribution for c quark and \bar{c} antiquark is convoluted with respective fragmentation functions simultaneously. As a result of the hadronization one obtains corresponding two-meson multidimensional distribution. In the last step experimental kinematical cuts on the distributions can be imposed. Then the resulting distributions can be compared with experimental ones. For numerical calculations here we again apply the Peterson model of fragmentation function [33].

The experimental cross sections for the production of two mesons are also (or even a bit more) sensitive to the details of hadronization as it was in the cases of the inclusive single D meson production discussed in the previous section. For example in Fig. 29 we compare transverse momentum distribution of D^0 meson provided that \bar{D}^0 is also measured for two different values of the ε_c parameter of the Peterson fragmentation function. The larger meson transverse momentum, the larger sensitivity to the value of ε_c . For illustration we show the range of transverse momenta relevant for the recent experiments of the LHCb collaboration [23]. The effect of the modification of the ε_c from 0.05 to 0.02 is quite sizeable. In the LHCb acceptance, it does not really affect the shape of calculated p_t distribution but has an important effect for the predictions of integrated cross sections. In Table II we compare measured by the LHCb collaboration cross sections for different $D\bar{D}$ modes with our theoretical results. Calculated values for three different UGDFs are consistent with the measured ones, taking into account rather large experimental and theoretical uncertainties. In particular, this is true only when $\varepsilon_c = 0.02$ is taken in the calculation of the fragmentation process. Results obtained with the KMR UGDF are the closest to the experimental numbers.

TABLE II: Integrated cross sections for the two mesons modes specified in the table below within the LHCb detector.

Mode	σ_{tot}^{EXP} [nb]	σ_{tot}^{THEORY} [nb]					
		KMR $^+(\mu)$ $^+(m_c)$		Jung setA+		KMS	
		$\varepsilon_c = 0.05$	$\varepsilon_c = 0.02$	$\varepsilon_c = 0.05$	$\varepsilon_c = 0.02$	$\varepsilon_c = 0.05$	$\varepsilon_c = 0.02$
$D^0\bar{D}^0$	$6230 \pm 120 \pm 630$	5193 $^{+1346}_{-879}$ $^{+654}_{-576}$	6971	4532	5814	2895	3894
$D^0 D^-$	$3990 \pm 90 \pm 500$	4155 $^{+1076}_{-704}$ $^{+523}_{-461}$	5577	3626	4652	2316	3115
$D^0 D_S^-$	$1680 \pm 110 \pm 240$	1471 $^{+381}_{-249}$ $^{+185}_{-163}$	1974	1284	1647	820	1103
$D^+ D^-$	$780 \pm 40 \pm 130$	831 $^{+215}_{-141}$ $^{+105}_{-92}$	1115	725	930	463	623
$D^+ D_S^-$	$550 \pm 60 \pm 90$	588 $^{+152}_{-99}$ $^{+74}_{-65}$	790	513	659	328	441
$D_S^+ D_S^-$	—	104 $^{+27}_{-17}$ $^{+13}_{-11}$	139	91	117	59	78

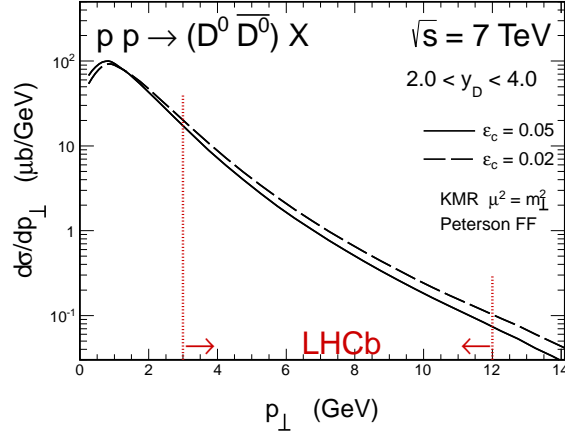


FIG. 29: Transverse momentum of D^0 meson within the LHCb acceptance provided that \bar{D}^0 was registered too. Here the KMR UGDF was used. We show results for different values of the Peterson fragmentation function parameter ε_c .

In Fig. 30 we present transverse momentum distributions of D^0 meson for the case when $D^0\bar{D}^0$ pairs are counted. We compare theoretical distributions for different UGDFs (left panel) as well as discuss effect of the scale dependence (right panel) on the shape of the p_t distribution. The experimental data points are normalized by a factor $1/\sigma$. The shape of the transverse momentum distribution is rather well reproduced by all used UGDFs. The normalization, as discussed already in Table II, is less consistent.

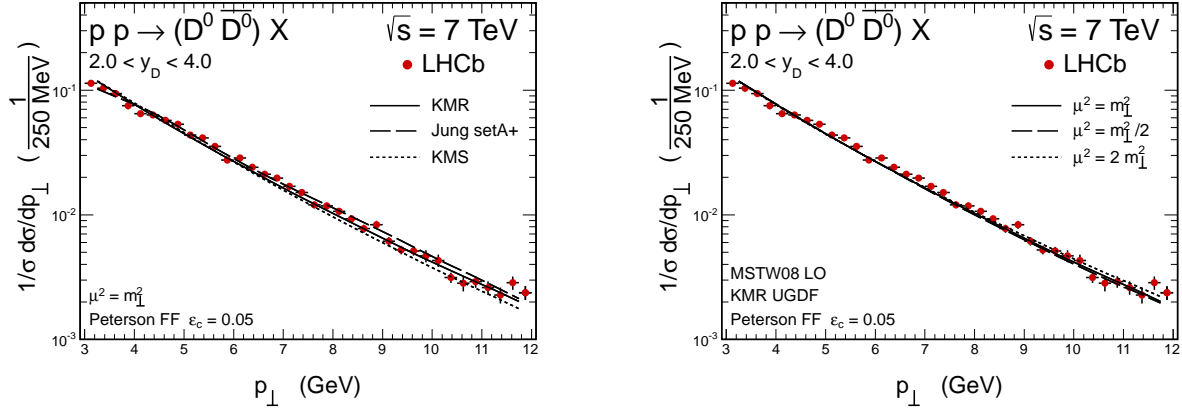


FIG. 30: Uncertainties for the conditional transverse momentum distribution due to the choice of UGDF model (left) and due to the choice of scales for the KMR UGDF (right). The experimental data of the LHCb collaboration are from Ref.[23].

The LHCb collaboration presented also distribution in the $D^0\bar{D}^0$ invariant mass $M_{D^0\bar{D}^0}$. In Fig. 31 we show the corresponding theoretical result for different UGDFs. Both, the KMR and KMS UGDFs provide the right shape of the distribution. The dip at small invariant masses is due to specific LHCb cuts on kinematical variables. On the other hand the shape of the distribution almost does not depend on the choice of the scales for the KMR UGDF

(see right panel).

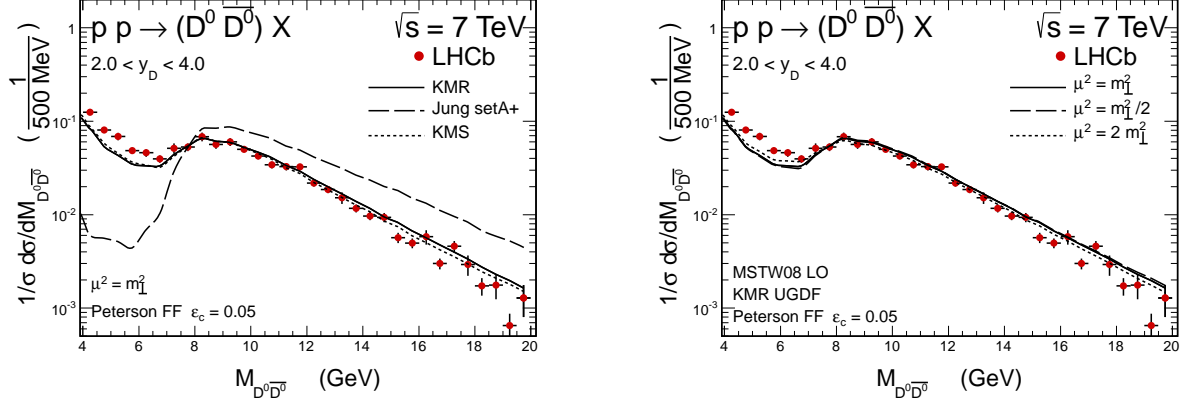


FIG. 31: Invariant mass distribution of the $D^0 \bar{D}^0$ system for different UGDFs (left) and uncertainties due to the choice of the scale for the KMR UGDF (right). The experimental data of the LHCb collaboration are taken from Ref. [23].

The LHCb detector has almost full coverage in azimuthal angle. In Fig. 32 we discuss distribution in azimuthal angle between the D^0 and \bar{D}^0 mesons $\varphi_{D^0 \bar{D}^0}$. Again the KMR and KMS distributions give quite reasonable description of the shape of the measured distribution. Both of them, give the enhancement of the cross section at $\phi_{D\bar{D}} \sim 0$. This is due to the fact that these approaches include effectively gluon splitting contribution, not included in the case of the Jung UGDFs. This was also discussed in Ref. [8] where additional calculations of the $g^* g^* \rightarrow gg \rightarrow g c \bar{c}$ subprocess in the case of the Jung UGDFs were performed to describe azimuthal angle correlation between D and \bar{D} mesons measured at Tevatron. Some dependence of the shape on the choice of the factorization/renormalization scale in the case of the KMR UGDF can be also observed (see the right panel). However, still even with the KMR UGDF, one can observe some small missing strenght at small angles. It may suggest that within the KMR model the gluon splitting contribution is not fully included.

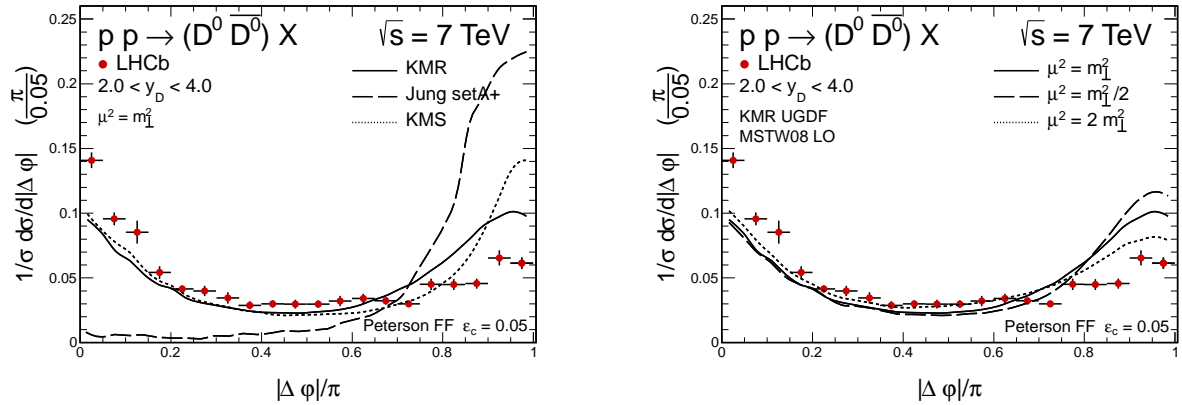


FIG. 32: Distribution in relative azimuthal angle between D^0 and \bar{D}^0 for different UGDFs (left) and uncertainties due to the choice of the scale for the KMR UGDF (right).

In order to better understand the result for the azimuthal correlations in Fig. 33 we show two-dimensional distributions in invariant mass $M_{D^0\bar{D}^0}$ and azimuthal angle between mesons $\varphi_{D^0\bar{D}^0}$. The maximum obtained for the KMR UGDF for small relative azimuthal angle between D and \bar{D} mesons corresponds to small invariant masses of the $D^0\bar{D}^0$ system. This strongly supports the interpretation of the effect as the gluon splitting into $c\bar{c}$ pair. However, one can also see that these interesting shapes of the correlation observable are the consequence of the specific LHCb kinematical cuts.

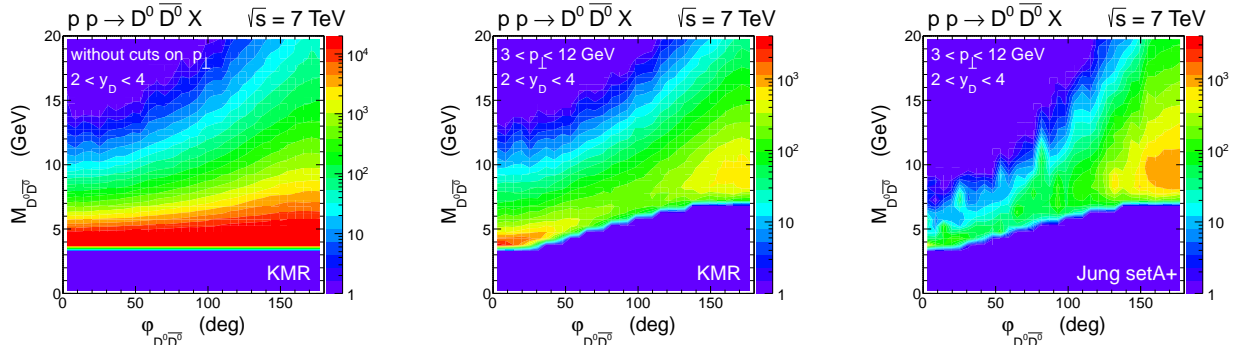


FIG. 33: Two-dimensional distribution in DD invariant mass and relative azimuthal angle between D and \bar{D} for the KMR and Jung setA+ UGDFs.

VI. SUMMARY

First we have discussed the general situation with the $c\bar{c}$ production at LHC energies. We have argued that the $c\bar{c}$ production is related with small- x physics. Therefore it has a good potential to test different models of unintegrated gluon distributions.

In the present paper we have focused on production of D mesons at the LHC within the k_t -factorization formalism with unintegrated gluon distributions. Only the Kimber-Martin-Ryskin unintegrated gluon distribution gives transverse momentum distributions of charmed mesons similar to the recently measured ones by the ATLAS, ALICE and LHCb collaborations. Our inclusive theoretical distributions with the KMR UGDFs are very similar to those obtained within FONLL or MC@NLO approaches. All other unintegrated gluon distributions strongly underpredict the experimental results. This may suggest that some mechanism of charm production is still missing. In a following paper we shall discuss double parton scattering effects as a potential missing mechanism [43].

Recently the LHCb collaboration has presented first results for D and \bar{D} meson two-particle distributions. We have presented first theoretical results for such observables. Our model calculation with the KMR UGDF relatively well describes both DD meson invariant mass distributions as well as DD correlations in relative azimuthal angle between meson and antimeson. This shows that the k_t -factorization approach is very efficient in describing the two-particle distributions. In contrast the NLO QCD approach can be used only in a limited region of the phase space but no real results have been presented so far in the literature.

Acknowledgments

We are indebted to Vanya Belyaev and Marek Szczekowski for the discussion concerning recent results at LHC. This study was partially supported by the Polish Grants DEC-2011/01/B/ST2/04535 and N202 237040.

-
- [1] P. Nason, S. Dawson and R.K. Ellis, Nucl. Phys. **B303** (1988) 607;
P. Nason, S. Dawson and R.K. Ellis, Nucl. Phys. **B327** (1989) 49;
W. Beenakker et al., Phys. Rev. **D 40** (1989) 54.
W. Beenakker et al., Nucl. Phys. **B351** (1991) 507.
 - [2] M. Cacciari, M. Greco and P. Nason, J. High Energy Phys. **05** (1998) 007;
M. Cacciari, S. Frixione and P. Nason, J. High Energy Phys. **03** (2001) 006.
 - [3] B. A. Kniehl, G. Kramer, I. Schienbein and H. Spiesberger, Phys. Rev. **D71** (2005) 014018;
Phys. Rev. Lett. **96** (2006) 012001; Phys. Rev. **D79** (2009) 094009.
 - [4] Ph. Hägler, R. Kirschner, A. Schäfer, I. Szymanowski and O.V Teryaev,
Phys. Rev. **D62** (2000) 071502.
 - [5] S.P. Baranov and M. Smizanska, Phys. Rev. **D62** (2000) 014012.
 - [6] S.P. Baranov, A.V. Lipatov and N.P. Zotov, Phys. Atom. Nucl. **67** (2004) 837;
Yad. Fiz. **67** (2004) 856.
 - [7] Yu.M. Shabelski and A.G. Shuvaev, Phys. Atom. Nucl. **69** (2006) 214.
 - [8] H. Jung, M. Kraemer, A.V. Lipatov and N.P. Zotov, J. High Energy Phys. **01** (2011) 085.
 - [9] H. Jung, M. Kraemer, A.V. Lipatov and N.P. Zotov, Phys. Rev. **D85** (2012) 034035;
 - [10] B.A. Kniehl, V.A. Saleev and A.V. Shipilova, Phys. Rev. **D79** (2009) 034007;
Phys. Rev. **D81** (2010) 094010.
 - [11] V.A. Saleev and A.V. Shipilova, Phys. Rev. **D86** (2012) 034032.
 - [12] M.A. Kimber, A.D. Martin and M.G. Ryskin, Phys. Rev. **D63** (2001) 114027;
G. Watt, A.D. Martin and M.G. Ryskin, Eur. Phys. J. **C31** (2003) 73.
 - [13] J. Kwieciński, A.D. Martin and A.M. Staśto, Phys. Rev. **D56** (1997) 3991.
 - [14] K. Kutak and A.M. Stasto, Eur. Phys. J **C41** (2005) 343.
 - [15] H. Jung, G.P. Salam, Eur. Phys. J. **C19** (2001) 351;
H. Jung, arXiv:0411287 [hep-ph].
 - [16] K. Golec-Biernat and M. Wusthoff, Phys. Rev. **D60** (1999) 114023-1.
 - [17] M. Łuszczak, R. Maciuła and A. Szczurek, Phys. Rev. **D79** (2009) 034009.
 - [18] R. Maciuła, A. Szczurek and G. Ślipek, Phys. Rev. **D83** (2011) 054014.
 - [19] The ATLAS collaboration, ATLAS-CONF-2011-017.
 - [20] B.I. Abelev et al. (The ALICE collaboration), J. High Energy Phys. **01** (2012) 128.
 - [21] The ALICE collaboration, CERN-PH-EP-2012-227; arXiv:1208.1948 [hep-ex].
 - [22] The LHCb collaboration, LHCb-CONF-2010-013.
 - [23] R. Aaij et al. (The LHCb collaboration), J. High Energy Phys. **06** (2012) 141.
 - [24] B.I. Abelev et al. (The STAR collaboration), Phys. Rev. Lett. **105** (2010) 202301;
A. Mischke, Phys. Lett. **B671** (2009) 361.
 - [25] J. Rademacker (The CDF collaboration), FERMILAB-CONF-07-634-E, Proceedings of Charm'07, Ithaca, NY, August 2007.
 - [26] S. Catani, M. Ciafaloni and F. Hautmann, Nucl. Phys. **366** (1991) 135.
 - [27] J.C. Collins and R.K. Ellis, Nucl. Phys. **B360** (1991) 3.
 - [28] R.D. Ball and R.K. Ellis, J. High Energy Phys. **05** (2001) 053.

- [29] M. Cacciari et al., J. High Energy Phys. **10** (2012) 137.
- [30] B.A. Kniehl et al., Eur. Phys. J. **C72** (2012) 2082.
- [31] M. Łuszczak and A. Szczurek, Phys. Rev. **D73** (2006) 054028.
- [32] S. Frixione and B.R. Webber, J. High Energy Phys. **06** (2002) 029.
- [33] C. Peterson, D. Schlatter, I. Schmitt, P.M. Zerwas, Phys. Rev. **D27** (1983) 105.
- [34] M. Cacciari, P. Nason and R. Vogt, Phys. Rev. Lett. **95** (2005) 122001.
- [35] E. Braaten et al., Phys. Rev. **D51** (1995) 4819.
- [36] V.G. Kartvelishvili et al., Phys. Lett. **B78** (1978) 615.
- [37] P.D.B. Collins and T.P. Spiller, Jour. Phys. G **11** (1985) 1289.
- [38] A.D. Martin, W.J. Stirling, R.S. Thorne and G. Watt, Eur. Phys. J. **C63** (2009) 189;
Eur. Phys. J. **C64** (2009) 653.
- [39] J. Pumplin et al., J. High Energy Phys. **07** (2002) 012;
H.L. Lai, Phys. Rev. **D82** (2010) 054021.
- [40] M. Glück, D. Jimenez-Delgado, E. Reya, Eur. Phys. J. **C53** (2008) 355.
- [41] M. Glück, E. Reya and A. Vogt, Eur. Phys. J. **C5** (1998) 461.
- [42] M. Łuszczak, R. Maciuła and A. Szczurek, Phys. Rev. **D84** (2011) 114018.
- [43] R. Maciuła and A. Szczurek, a paper in preparation.